Bioorganic Chemistry 40 (2012) 99–107

Contents lists available at SciVerse ScienceDirect

Bioorganic Chemistry

journal homepage: www.elsevier.com/locate/bioorg

Density functional calculations on the effect of sulfur substitution for 2′-hydroxypropyl-p-nitrophenyl phosphate: C—O vs. P—O bond cleavage

Futing Xia [a], Hua Zhu [a,b,*]

[a] School of Chemistry, Sichuan University, Chengdu 610064, China
[b] State Key Laboratory of Biotherapy, Sichuan University, Chengdu 610064, China

ARTICLE INFO

Article history:
Received 24 August 2011
Available online 17 September 2011

Keywords:
2′-Hydroxypropyl-p-nitrophenyl phosphate
2-Thiouridyl-p-nitrophenyl phosphate
Intra-molecular attack
Polarized continuum model
DFT

ABSTRACT

Density functional theory calculations have been used to investigate the intra-molecular attack of 2′-hydroxypropyl-p-nitrophenyl phosphate (HPpNP) and its analogous compound 2-thiouridyl-p-nitrophenyl phosphate (s-2′pNP). Bulk solvent effect has been tested at the geometry optimization level with the polarized continuum model. It is found that the P-path involving the intra-molecular attack at the phosphorus atom and C-path involving the attack at the beta carbon atom proceed through the S_N2-type mechanism for HPpNP and s-2′pNP. The calculated results indicate that the P-path with the free energy barrier of about 11 kcal/mol is more accessible than the C-path for the intra-molecular attack of HPpNP, which favors the formation of the five-membered phosphate diester. While for s-2′pNP, the C-path with the free energy barrier of about 21 kcal/mol proceeds more favorably than the P-path. The calculated energy barriers of the favorable pathways for HPpNP and s-2′pNP are both in agreement with the experimental results.

1. Introduction

Phosphoryl transfer reactions and the hydrolysis of phosphate esters have attracted considerable attention as they are involved in many biological processes [1–3]. The phosphodiester is the backbone of DNA and RNA, and the hydrolysis rate of RNA is 100 faster than that of DNA under room temperature. The reason for this difference lies in the intra-molecular attack by the 2′ hydroxyl group on the phosphorus atom of RNA to form the five-membered cyclic phosphodiesters, making the cleavage of RNA much easier. Up to now a series of RNA analogs have been used to investigate the intra-molecular attack [4–10]. Among various phosphate esters, 2′-hydroxypropyl-p-nitrophenyl phosphate (HPpNP, see Scheme 1) is the mostly used model to study the RNA cleavage reaction [5–11] since the p-nitrophenol group activates the phosphate center toward the nucleophile and makes it more convenient to follow the transphosphorylation reaction [5].

A variety of experimental [15,11–23] and theoretical [24–44] work has been devoted to the transphosphorylation and hydrolysis of phosphate esters with P—O bond cleavage. One of the open questions on the reactivity of phosphate esters is whether the nucleophilic attack of phosphoryl transfer and phosphates hydrolysis proceeds through an associative or dissociative mechanism [15,18,29]. It has been suggested that the hydrolysis of the monoesters proceed by a dissociative pathway containing a complete bond cleavage to the leaving group and no bond formation to the nucleophile [14,17,18,45]. For the diesters with aryl leaving groups, it undergoes hydrolysis via a concerted pathway with a tighter transition state [12,13,16,19]. Phosphotriesters react through an associative reaction that involve the phosphorane intermediate with no bond cleavage to the leaving group and complete bond formation to the nucleophile [20,22,36]. The experimental work indicated that the transition states for the nucleophilic process of some phosphate within or without enzyme are similar [21,22]. A deeper understanding for the nonenzymatic reaction of the HPpNP should provide fundamental microscopic insights into the RNA cleavage mechanisms [33,41].

Despite the vast majority of the publications reported on the nucleophilic attack with P—O bond cleavage, phosphate esters also proceed through C—O bond cleavage reaction [31,46–55]. It was reported early in 1965 that the different ester group would get the products with P—O or C—O bond cleavage for the hydrolysis of hydroxyalkyl phosphate esters [47]. In 1992, Lum et al. found that except for the methoxide-d and ethoxide, several other anionic nucleophiles reacting with trimethyl phosphate (TMP) yielded products with C—O bond cleavage in the gas phase [50]. An ab initio study of the thiolysis of TMP in the gas phase performed by Menegon, G. et al. suggested that the thiomethoxide attack at TMP carbon was more favorable than the attack at phosphorus [31]. Subsequently, it was found that the phosphate monoester tetrahedral

* Corresponding author at: School of Chemistry, Sichuan University, Chengdu 610064, China.
E-mail address: zhuhua@scu.edu.cn (H. Zhu).

0045-2068/$ - see front matter Crown Copyright © 2011 Published by Elsevier Inc. All rights reserved.
doi:10.1016/j.bioorg.2011.09.003

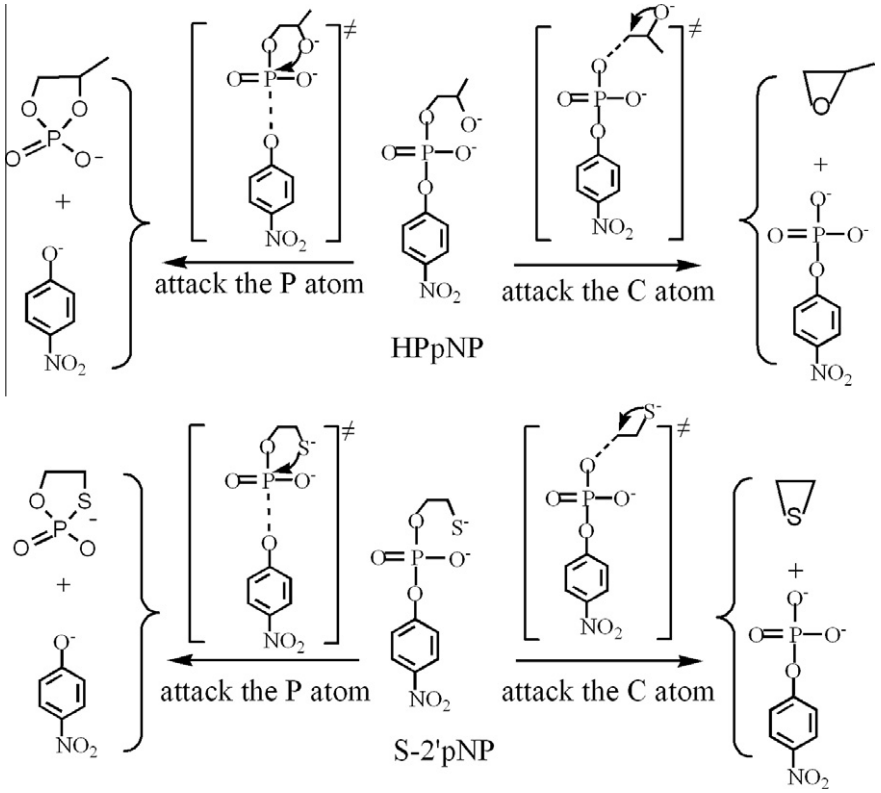

Scheme 1. P—O and C—O bond cleavage reaction for HPpNP and s-2′pNP.

intermediate (THI) broke down exclusively through C—O bond cleavage [52,53]. A further investigation of the selective site controlled nucleophilic attack with P—O or C—O bond cleavage on 2-alkoxy-1,3,2-dioxaphospholane-2-oxide with various nucleophiles was carried out by Ashkenazi et al., and the results indicated that the 5-membered ring phosphate triesters exhibited dual electrophilic character [54,55].

For the diester HPpNP, the experimental work demonstrates that it proceeds through nucleophilic reaction at the phosphorus atom with P—O bond cleavage, undergoing facile cyclization and elimination of p-nitrophenol [47]. However, when the sulfur atom substitutes the nucleophilic position, 2-thiouridyl-p-nitrophenyl phosphate (s-2′pNP), the sulfur atom attacks at the beta carbon atom, with the forming of thiirane and a phosphomonoester undergoes C—O bond cleavage [56]. Many previous publications [3,57–60] have reported on the sulfur substitution of the phosphoryl transfer and the hydrolysis of phosphate esters, and showed the substitution of oxygen atom by sulfur atom would change the rate constants and mechanisms of the reactions. For HPpNP, the sulfur substitution on the nucleophilic position leads to intramolecular attack at the different site. The intriguing phenomena inspires us to probe into the different reactivity of HPpNP and s-2′pNP. The uncertainty of understanding the mechanism of intra-molecular attack of HPpNP and s-2′pNP warrants detailed theoretical studies on such reactions as not much effort has been made in this direction, especially for the C—O bond cleavage reactions. In the present work, two density functional methods (B3LYP and B3PW91) are used to study the intra-molecular attack mechanism for HPpNP and s-2′pNP. Both P—O and C—O bond cleavage reaction pathways, named P-path and C-path respectively, are taken into account for HPpNP and s-2′pNP (Scheme 1). The effect of solvent is considered within an implicit polarizable continuum model (PCM) in our calculations. Full geometry optimizations with PCM of the stationary states are performed to map out the reaction pathways for HPpNP and s-2′pNP.

2. Computational details

Geometries of the reactants, transition states and products for the reaction of HPpNP and s-2′pNP were fully optimized at the density functional theory (DFT) B3LYP/6-31++G(df,p) and B3PW91/6-31++G(df,p) levels. The Becke three parameter exchange functional and the gradient-corrected functional of Lee, Yang, and Parr (B3LYP) [61,62], as well as the hybrid Becke three parameter Perdew–Wang 1991 (B3PW91) [63,64] functionals have been successfully applied in the transphosphorylation and hydrolysis of phosphate and other analogous systems [30,38–40,53]. The use of diffuse functions is crucial to describe properly the diffuse nature of anions. The nature of the stationary points was confirmed by the harmonic frequency analysis as a minimum with all positive frequencies or as a transition state with only one imaginary frequency. The intrinsic reaction coordinate (IRC) calculations [65,66] were performed from all the transition states to verify the connectivity between the stationary points. Zero-point vibration energy (ZPVE) corrections, enthalpy corrections and Gibbs free energy corrections to the total energy were carried out based on the frequency calculations at the B3LYP/6-31++G(df,p) and B3PW91/6-31++G(df,p) levels.

In view of the fact that the intra-molecular attack reactions actually take place in solution, it is of great significance to study the influence of solvent water on the reactions. The calculations made by Kameline et al. indicated that the results with the implicit solvent model is convincing dealing with the hydrolysis of phosphate diesters [42]. We further optimized the geometries of the stationary points in water at the B3LYP/6-31++G(df,p) and B3PW91/6-31++G(df,p) level together with the polarized continuum model

PCM [67] with ε = 78.4. Furthermore, geometries optimized at the B3LYP/6-31++G(df,p) and B3PW91/6-31++G(df,p) level in solution phase were employed for energy evaluation using larger basis sets 6-311++G(3df,2pd) with PCM to obtain more credible energy information. In order to further understand the various bond-breaking and bond-making processes, we calculated the Wiberg bond indexes [68] using the natural bond orbitalal NBO program [69] at the B3LYP/6-31++G(df,p) level for the structures obtained in solution. All calculations were performed by Gaussian 03 [70] programs.

3. Results and discussion

The main structural and energetic features of the intra-molecular attack of HPpNP and s-2′pNP are presented in this section. To facilitate the identification of each transition state and complex, we adopt a nomenclature to characterize each stationary point in the following pathways. The subscripts P and C identify whether the nucleophilic attack takes place at the phosphorus or beta carbon atom. For example, **O-TS$_P$** stands for the transition state of the nucleophilic attack taking place at the P atom for HPpNP, whereas **S-TS$_C$** stands for the transition state of the nucleophilic attack taking place at the beta C atom for s-2′pNP.

All the geometric structures were optimized at the B3LYP/6-31++G(df,p) and B3PW91/6-31++G(df,p) levels both in the gas phase and in solution. The related geometric parameters are similar in the gas phase and in solution with two DFT methods (Table 1). In the present work, the following discussions are mainly based on the geometries optimized at the B3LYP/6-31++G(df,p) level in solution.

3.1. Intra-molecular attack of HPpNP

Kinetic data on the intra-molecular reaction of HPpNP implies that the nucleophile is deprotonated in a pre-equilibrium step before nucleophilic attack and no proton is in flight in the rate-determining step [71]. Obviously, nucleophile is deprotonated more easily in the pre-equilibrium step with the increase of pH. In the present work, it is our interest to study the rate-determining step with the nucleophilic attack by ignoring the deprotonation step.

The optimized geometries for the intra-molecular attack of HPpNP and important bond lengths and angles for the stationary points at B3LYP/6-31++G(df,p) in solution are shown in Fig. 1. Cartesian coordinates optimized in water are given in the Supporting information.

3.1.1. P-path

As described in Fig. 1a, two isomers of HPpNP **O-RE$_1$** and **O-RE$_2$** are located on the free energy profile. In the first process, we found that the $O_{2'}$ atom can rotate around the C_α—C_β bond to make the $O_{2'}$ atom fit to interact with the P_1 atom through the transition state **O-TSR**. For **O-TSR**, the bond lengths of all bonds are very close to those of **O-RE$_1$**, except that the $O_{2'}$—C_α—C_β—$O_{3'}$ dihedral angel changes from 175.5° in **O-RE$_1$** to116.5° in **O-TSR**, showing that

Table 1
Selected geometrical parameters (bond distances in Å, and angle in deg) of the stationary points for the intramolecular attack of HPpNP and s-2′pNP for the P-path and the C-path in the gas phase and in solution (PCM) at the B3LYP/6-31++G(df,p) level, the values in parentheses are at the B3PW91/6-31++G(df,p) level.

	GAS			PCM		
	$O_{2'}$—P_1	P_1—$O_{5'}$	$O_{2'}$—P_1—$O_{5'}$	$O_{2'}$—P_1	P_1—$O_{5'}$	$O_{2'}$—P_1—$O_{5'}$
O–P path						
O-RE$_1$	5.066	1.780	93.3	5.052	1.694	94.9
	(5.045)	(1.769)	(92.9)	(5.026)	(1.689)	(94.8)
O-TSR	4.854	1.779	102.6	4.821	1.692	106.4
	(4.840)	(1.768)	(102.2)	(4.801)	(1.687)	(106.7)
O-RE$_2$	4.615	1.770	104.7	4.452	1.694	111.2
	(4.597)	(1.772)	(104.5)	(4.434)	(1.689)	(110.9)
O-TS$_P$	2.709	1.984	158.8	2.472	1.801	163.7
	(2.720)	(1.929)	(158.8)	(2.524)	(1.780)	(163.0)
O-MEP$_P$	1.696			1.654		
	(1.691)			(1.649)		
O–C path						
	$O_{2'}$—C_β	C_β—$O_{3'}$	$O_{2'}$—C_β—$O_{3'}$	$O_{2'}$—C_β	C_β—$O_{3'}$	$O_{2'}$—C_β—$O_{3'}$
O-RE$_1$	2.382	1.466	144.3	2.386	1.459	144.0
	(2.377)	(1.455)	(144.3)	(2.378)	(1.449)	(144.0)
O-TS$_C$	1.880	2.059	155.9	1.909	2.008	157.2
	(1.861)	(2.027)	(156.6)	(1.888)	(1.978)	(158.0)
O-PC$_C$	1.462	4.073	121.6	1.452	4.091	85.8
	(1.448)	(3.995)	(125.2)	(1.440)	(4.136)	(85.6)
S–P path						
	$S_{2'}$—P_1	P_1—$O_{5'}$	$S_{2'}$—P_1—$O_{5'}$	$S_{2'}$—P_1	P_1—$O_{5'}$	$S_{2'}$—P_1—$O_{5'}$
S-RE	5.515	1.771	90.4	5.470	1.690	89.5
	(5.489)	(1.762)	(91.1)	(5.434)	(1.685)	(90.8)
S-TS$_P$	3.164	2.357	155.6	2.580	2.109	164.4
	(3.009)	(2.202)	(158.5)	(2.507)	(2.063)	(164.9)
S-sEP$_P$	2.245			2.178		
	(2.224)			(2.164)		
S–C path						
	$S_{2'}$—C_β	C_β—$O_{3'}$	$S_{2'}$—C_β—$O_{3'}$	$S_{2'}$—C_β	C_β—$O_{3'}$	$S_{2'}$—C_β—$O_{3'}$
S-RE	2.815	1.464	146.1	2.790	1.458	146.9
	(2.795)	(1.455)	(146.4)	(2.773)	(1.448)	(147.0)
S-TS$_C$	2.196	2.190	158.1	2.262	2.081	159.0
	(2.175)	(2.146)	(158.5)	(2.230)	(2.053)	(159.5)
S-PC$_C$	1.862	3.691	102.6	1.852	3.963	92.1
	(1.863)	(2.996)	(164.0)	(1.835)	(3.965)	(91.8)

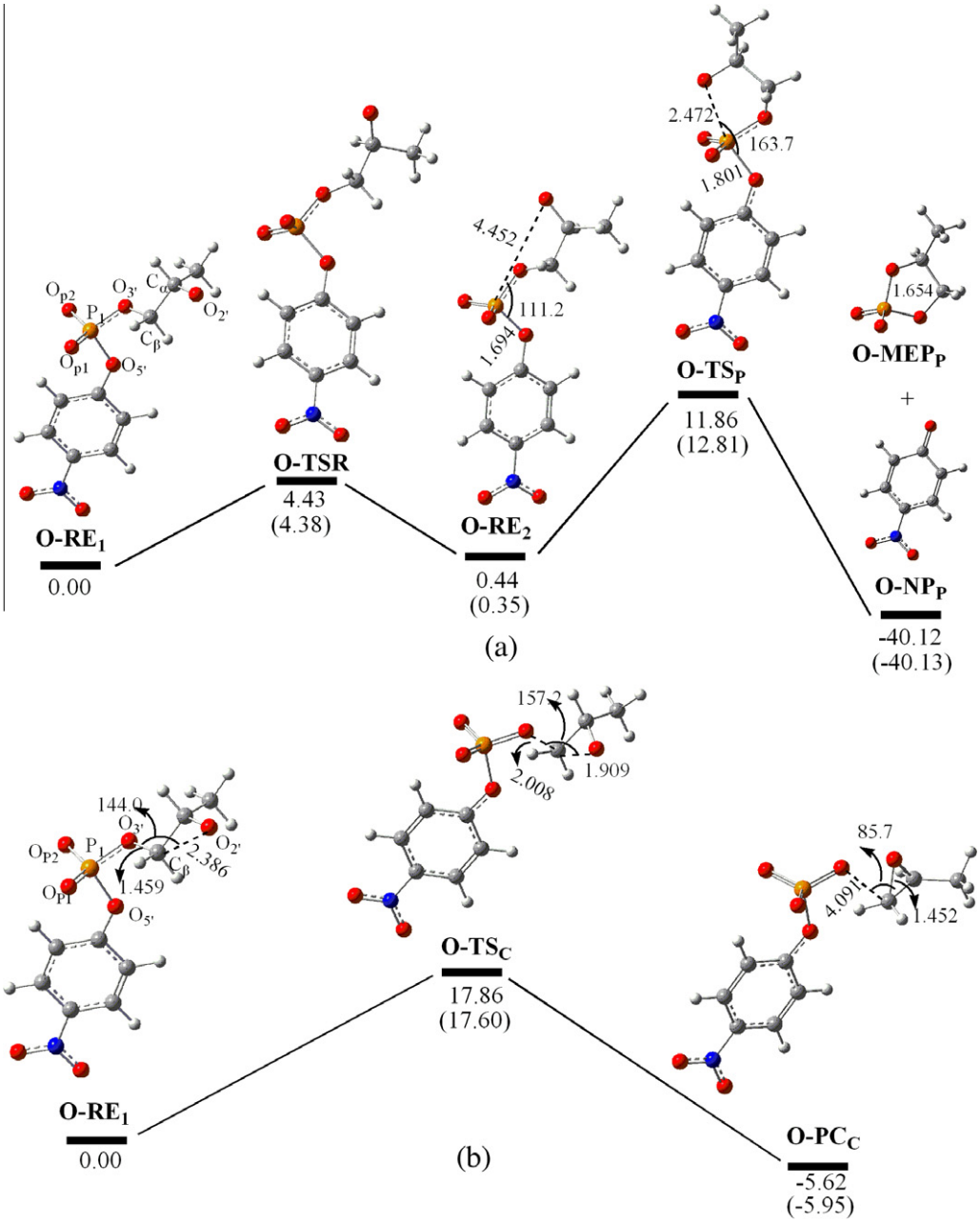

Fig. 1. B3LYP/6-31++G(df,p)-optimized structures (in Å) of the stationary points of HPpNP in the solution for the P-path (a) and the C-path (b), respectively. The values correspond to the relative free energy (ΔG) in kilocalories per mole. The values in parentheses are at the B3LYP/6-311++G(3df,2pd)//B3LYP/6-31++G(df,p) level.

O-TSR is a rotational transition state. The imaginary frequency of **O-TSR** is 91.92 i cm^{-1}. The analysis of the vibration modes indicates that this imaginary frequency is exactly associated with the C_α—C_β bond rotary motion. The low free energy barrier (4.43 kcal/mol) for this process shows that the isomerization of HPpNP with C_α—C_β bond rotary motion can easily occur. After the reaction surmounted the transition state **O-TSR**, **O-RE$_2$** (the Gibbs free energy in solution is 0.44 kcal/mol) is formed and it is slightly less stable than the **O-RE$_1$**. For **O-RE$_2$,** although the bond distances of all the bonds are also close to those of **O-RE$_1$**, the $O_{2'}$—C_α—C_β—$O_{3'}$ dihedral angel changes to 65.3°.

In the following process, a unique trigonal bipyramidal (TBP) transition state **O-TS$_P$**, which is directly connected to **O-RE$_2$** and the products, has been located as depicted in Fig. 1a. **O-TS$_P$** has only one imaginary frequency of 155.47 i cm^{-1}. The analysis of the vibration modes identify that the imaginary frequency is associated with the shortening motion of the $O_{2'}$—P_1 and stretching motion of the P_1—$O_{5'}$ bond. As shown in Fig. 1a, the $O_{2'}$—P_1 atomic distance is 2.472 Å in **O-TS$_P$**, nearly 2 Å shorter than that of **O-RE$_2$** and the $O_{2'}$—P_1 Wiberg bond indices for **O-RE$_2$** and **O-TS$_P$** are 0.002 and 0.143 respectively. The bond length of P_1—$O_{5'}$ in **O-TS$_P$** is about 0.1 Å longer than that of **O-RE$_2$** and the **P_1—$O_{5'}$** Wiberg bond indices for **O-RE$_2$** and **O-TS$_P$** are 0.486 and 0.389, respectively. These changes reveal that **O-TS$_P$** has the trend to generate the product **O-MEP$_P$** and **O-NP$_P$**. The concerted transition state **O-TS$_P$** has a slightly elongated P=O double bond 1.512 vs. 1.508 Å in the **O-RE$_2$**, apparently as a result of the weakening of the double bond. The angle of $O_{2'}$—P_1—$O_{5'}$ is 163.7° in **O-TS$_P$** indicating that the attacking and leaving groups is in axial position and this process proceeds via a nearly in-line nucleophilic displacement.

In the current calculations starting from **O-TS$_P$**, the IRC calculation in the forward direction clearly pointed to the separated prod-

ucts. We failed to get the converged geometries for product complex in this pathway. This is understandable, because there is strong coulomb repulsion between the two anionic species p-nitrophenol (NP) and methyl-ethylene phosphate (MEP). Consequently, the P_1—$O_{5'}$ Wiberg bond index in the product complex is set as 0.000 in our discussion. The $O_{2'}$—P_1 Wiberg bond index for **O-MEP$_P$** is 0.586, indicating the formation of the final product.

Accordingly, the P-path of HPpNP involves both the addition and elimination coordinates and has a one-step S_N2-like mechanism without formation of an intermediate. The result is in accord with the previous Linear free energy relationships (LFER) [12,13] and kinetic isotope effects [16,19,72] studies, which have shown that the diesters with aryl leaving groups undergo hydrolysis via a concerted pathway.

Based on the calculated Wiberg bond indexes for the structures optimized in solution at the B3LYP/6-31++G(df,p) level, B_i is the bond order and the superscripts RC, TS and PC denote the reactant complex, transition state and product complex, respectively. E_v (%) stands for the relative evolution of the bond order, which is expressed as

$$E_v\ (\%) = \frac{B_i^{TS} - B_i^{RC}}{B_i^{PC} - B_i^{RC}} \quad (1)$$

Synchronicity (S_y), proposed by Moyano et al. [73] describes the global nature of bond breaking and making processes involved in the reaction pathway monitored above. S_y is defined as

$$S_y = 1 - \frac{\sum_{i=1}^{n} \frac{|[(E_v)_i\ (\%)] - [(E_{av})_i\ (\%)]|}{(E_{av})_i\ (\%)}}{2n-2} \quad (2)$$

where n refers to the number of bonds directly involved in one step of the reaction and E_{av}(%) refers to the average percentage of evolution of the bond orders. It is obvious that S_y is less than 1.00 and a larger synchronicity value indicates the strong synchronicity.

E_v (%), E_{av} (%) and synchronicity (S_y) for the reactions are presented in Table 3. In the P-path for HPpNP, the nucleophilic attack, the formation of $O_{2'}$—P_1 is the most advanced, 24%, while the bond-breaking P_1—$O_{5'}$ bond is slightly later. The cyclization of HpPNP has a transition state with greater nucleophilic participation than the bond breaking to the leaving group was showed by Kinetic isotope effects (KIEs) measured in the nucleophilic atom and in the leaving group [74]. The percentage of evolution of bond orders implies a somewhat early transition state. A concerted transition state may be either synchronous, where the amounts of bonding to the nucleophile and the leaving group are roughly equal, or asynchronous. An asynchronous transition state can be either associative, with more bond formation to the nucleophile than the bond breaking to the leaving group, or dissociative, with a larger degree of bond breaking than bond formation. The E_v(%) of bond formation and bond breaking (24.14% and 19.95%) indicates the concerted transition state can be roughly viewed as synchronous or a little associative. The synchronicity value 0.90 shows that this pathway closes to a synchronous process.

3.1.2. C-path

Further searches for the unimolecular decomposition reaction reveal the second possible transition state, where the $O_{2'}$ atom attacks the beta carbon atom (C_β) of HPpNP. All the optimized structures of the reactants, transition states, and products for this pathway are presented in Fig. 1b.

In the **O-RE$_1$**, the nucleophilic $O_{2'}$ keeps close to the C_β, the $O_{2'}$—C_β distance 2.386 (Å) being about 2 Å shorter than that $O_{2'}$—P_1 bond in **O-RE$_2$** 4.452 (Å). When the attacking $O_{2'}$ atom approaches the C_β atom, a transition state, **O-TS$_C$** emerges along the potential energy profile. The calculated imaginary frequency of 502.62 i cm^{-1} together with its vibrational mode signifies a strong interaction between the nucleophilic $O_{2'}$ and the C_β atom. An analysis of the vibrational modes indicates that **O-TS$_C$** connects exactly with **O-RE$_1$** and **O-PC$_C$**. In **O-RE$_1$**, the distance between the $O_{2'}$ and the C_β atoms is larger than 2.0 Å, whereas in **O-TS$_C$**, as shown in Fig. 1b, the $O_{2'}$—C_β bond distance shorten to 1.909 Å and the corresponding Wiberg bond indices increase from 0.069 Å in **O-RE$_1$** to 0.458 Å in **O-TS$_C$**. The bond lengths of C_β—$O_{3'}$ in **O-RE$_1$** and **O-TS$_C$** are 1.459 and 2.008 Å, and the Wiberg bond indices for them are 0.846 and 0.366, respectively.

Passing through such a transition state, the final reaction product **O-PC$_C$** is produced. **O-PC$_C$** is a complex of p-Nitrophenyl Phosphate (pNPP) and methyl-ethylene oxide characterized by the C_β—$O_{3'}$ distance of 4.091 Å, which increased by 2.09 Å compared to that of the **O-TS$_C$**. The $O_{2'}$—C_β of **O-PC$_C$** distance is 1.452 Å, nearly equal to the C_β—$O_{3'}$ distance 1.459 in **O-RE$_1$**. The Wiberg bond indices for the C_β—$O_{3'}$ and $O_{2'}$—C_β bond are 0.001 Å and 0.902 Å, respectively. The large bond distances and small Wiberg bond indices on the C_β—$O_{3'}$ bond show that the C_β—$O_{3'}$ bond has broken completely. The small bond distances and large Wiberg bond indices on the $O_{2'}$—C_β bond indicates that the $O_{2'}$—C_β bond has formed completely. With the formation of the final product, the nucleophilic attack from the back side of the carbon atom is completely accomplished. Apparently, the macrocyclization occurs by S_N2 intra-molecular displacement. Only backside-attack S_N2 reaction is considered in our work as the regular backside-attack S_N2 reaction at the carbon atom has a lower reaction barrier than the corresponding frontside pathway [75].

E_v (%), E_{av} (%) and synchronicity (S_y) for the C-path are presented in Table 3. In the C-path for HPpNP, the C_β—$O_{3'}$ bond-breaking are more advanced than $O_{2'}$—C_β bond-attacking. The E_v(%) values 46–57% for the C-path are more advanced than that of the P-path with the E_v(%) about 20%. It implies that the transition state for the C-path is later than the P-path. The synchronicity value is 0.90 showing that the C-path for the HPpNP can also be viewed as a synchronous process.

3.1.3. Energy profile

The changes in energy including zero-point vibrational energy (ΔE_0), enthalpy of activation (ΔH) and Gibbs free energies (ΔG) for all the stationary points of HPpNP with respect to the reactant **O-RE$_1$** are given in Table 2.

For the P-path of HPpNP, there is a rotational transition state **O-TSR** with the free energy barrier of 4.43 kcal/mol on the free energy profile. The low free energy barrier for this process shows that the isomerization of HPpNP directly connected to **O-RE$_1$** and **O-RE$_2$** can easily occur. **O-RE$_2$** (the Gibbs free energy in solution is 0.44 kcal/mol) is slightly less stable than the **O-RE$_1$**. In the next step, ΔE_0 and ΔG of **O-TS$_P$** are 15.40 and 17.09 kcal/mol, respectively in the gas phase. The entropic contributions tend to increase the energy barrier, the free energy barriers ascending about 1 kcal/mol in the P-path. Both the ΔE_0 and ΔG at the B3PW91/6-31++G(df,p) are slightly lower than that at the B3LYP/6-31++G(df,p) level. The bulk solvent effects are not small on the energy barrier of the pathway. For example, the free energy barrier of the P-path is 11.86 kcal/mol in solution, about 5 kcal/mol lower than that in the gas phase at B3LYP/6-31++G(df,p) level. Correspondingly, the free energy barrier is 10.65 kcal/mol in solution, about 6 kcal/mol lower than that in the gas phase at B3PW91/6-31++G(df,p) level. When the single point energies were recalculated with PCM at the B3LYP/6-311++g(3df,2pd) level, the ΔE_0 and ΔG become about 1 kcal/mol higher than the energies obtained with PCM at B3LYP/6-31++G(df,p) level. The ΔG of **O-TS$_P$** is about 12 kal/mol in solution, and it is close to that measured by Gregersen et al. with QM/MM methods (10.5 kal/mol) [32]. The E_a derived from ΔH of O-TS_P for the P-path of HPpNP is about

Table 2
Relative energies (in kcal/mol) with respect to the reactant (RE) for the intramolecular attack of HPpNP and s-2′pNP for the P-path and the C-path in the gas phase and in solution (PCM) at the B3LYP/6-31++G(df,p) and B3PW91/6-31++G(df,p) level. The values in parentheses are at the B3LYP/6-311++G(3df,2pd)//B3LYP/6-31++G(df,p) or B3PW91/6-311++G(3df,2pd)//B3PW91/6-31++G (df,p) level.

	GAS						PCM					
	B3LYP			B3PW91			B3LYP			B3PW91		
	ΔH	ΔE_0	ΔG	ΔH	ΔE_0	ΔG	ΔH	ΔE_0	ΔG	ΔH	ΔE_0	ΔG
O–P path												
O-TSR	4.78	5.33	6.82	4.674	5.22	6.59	3.26	3.75	4.43	3.29	3.77	4.26
							(3.21)	(3.70)	(4.38)	(3.24)	(3.71)	(4.21)
O-RE_2	3.92	3.92	4.55	4.293	4.34	4.97	0.42	0.43	0.44	0.35	0.35	0.30
							(0.33)	(0.33)	(0.35)	(0.26)	(0.26)	(0.21)
O-TS_P	14.99	15.40	17.09	14.57	15.03	16.82	9.52	10.12	11.86	8.30	8.91	10.65
							(10.47)	(11.07)	(12.81)	(9.24)	(9.85)	(11.59)
O-MEP_P + O-NP_P	−75.43	−74.69	−84.95	−77.80	−77.07	−87.65	−29.74	−29.11	−40.12	−31.62	−30.98	−42.05
							(−29.75)	(−29.12)	(−40.13)	(−31.56)	(−30.93)	(−42.00)
O–C path												
O-TS_C	11.58	17.36	17.11	18.59	18.42	18.12	18.60	18.43	17.86	19.56	19.41	18.91
							(18.34)	(18.17)	(17.60)	(19.43)	(19.28)	(18.78)
O-PC_C	6.02	5.19	2.96	5.79	5.08	3.18	−0.61	−1.53	−5.62	−2.46	−2.27	−3.53
							(−0.94)	(−1.86)	(−5.95)	(−2.76)	(−2.57)	(−3.83)
S–P path												
S-TS_P	24.05	24.19	24.40	24.15	24.46	25.54	23.13	23.52	25.02	21.23	21.65	23.08
							(23.71)	(24.09)	(25.59)	(21.70)	(22.10)	(23.54)
S-sEP_P + S-NP_P	−46.63	−46.01	−56.38	−49.32	−48.66	−58.56	−1.59	−1.02	−11.60	−3.33	−2.76	−13.54
							(−1.43)	(−0.86)	(−11.45)	(−3.54)	(−2.98)	(−13.75)
S–C path												
S-TS_C	20.99	20.71	19.82	21.99	21.81	21.62	20.75	20.61	20.31	22.03	21.89	21.33
							(20.22)	(20.07)	(19.77)	(21.50)	(21.35)	(20.79)
S-PC_C	15.83	15.06	13.07	17.49	16.70	14.41	7.63	6.89	4.64	7.82	7.05	4.48
							(7.04)	(6.30)	(4.05)	(7.12)	(6.35)	(3.77)

Table 3
Wiberg bond indexes (B_i), percentage of evolution of bond order ($\%E_v$) and synchronicity (S_y)[73] at B3LYP/6-31++G(df,p) in solution.

	Bond	B_i^{RC}	B_i^{TS}	B_i^{PC}	$\%E_v$	$\%E_{v(av)}$	S_y
O–P path							
RE → TS → MEP + NP	$O_{2'}$—P_1	0.002	0.143	0.586	24.14	22.04	0.90
	P_1—$O_{5'}$	0.486	0.389	0.000	19.95		
O–C path							
RE → TS → PC	$O_{2'}$—C_β	0.069	0.458	0.902	46.70	51.75	0.90
	C_β—$O_{3'}$	0.846	0.366	0.001	56.80		
S–P path							
RE → TS → sEP + NP	$S_{2'}$—P_1	0.003	0.385	0.736	52.11	53.70	0.97
	P_1—$O_{5'}$	0.492	0.220	0.000	55.28		
S–Cpath							
RE → TS → PC	$S_{2'}$—C_β	0.051	0.483	0.960	47.52	54.07	0.88
	C_β—$O_{3'}$	0.844	0.333	0.001	60.62		

10 kcal/mol, which is very close to the experimental value 10.5 kcal/mol [47].

For the C-path of HPpNP, the energy barrier is 17.36 kcal/mol and the free energy barrier is 17.11 kcal/mol in the gas phase. The entropic contributions tend to decrease the energy barrier. Both the ΔE_0 and ΔG at the B3PW91/6-31++G(df,p) are about 1 kcal/mol higher than that at the B3LYP/6-31++G(df,p) level. The bulk solvent effects increase the energy barrier of the C-path slightly. The ΔE_0 and ΔG in solution are higher than that in the gas phase at B3LYP/6-31++G(df,p) and B3PW91/6-31++G(df,p) levels. Contrary to those of the P-path, when the single point energy were recalculated at B3LYP/6-311++g(3df,2pd) and B3PW91/6-311++g(3df,2pd) levels, the ΔE_0 and ΔG become slightly lower. Geometries optimized at the B3LYP/6-31++G(df,p) level were further employed for energy evaluation in solution using second order Møller–Plesset (MP2) theory [76,77]. The MP2 method increases the free energy barriers of two pathways, and the free energy barriers ΔG for the P-path and C-path of HPpNP are 15.98 and 25.00 kcal/mol, respectively.

Our results indicated the P-path, where the nucleophilic attack takes place at the phosphorus atom with P—O bond cleavage, is more favorable than the C-path with the attack at the carbon atom with C—O bond cleavage for HPpNP. One can further infer that the 2′ hydroxyl group intra-molecular attack favors the formation of the products with the five-membered phosphate diester and p-nitrophenol characterized by P—O bond cleavage for HPpNP. Actually, the experimental work showed HPpNP proceeds through nucleophilic reaction at the phosphorus atom with P—O bond cleavage, undergoing facile cyclization and elimination of p-nitrophenol [47].

Further calculations on the charge and the orbitalal properties were performed in order to get more insights for the reactivity of HPpNP. The Natural Population Analysis (NPA) charge distribution from NBO (natural bond orbital) method for the reactant is presented in Table 1-SI. The NPA charge carried by the $O_{2'}$, P_1 and C_β atom is about −0.90e, 2.57e, −0.11e, respectively for **O-RE_2** and **O-RE_1**. Apparently, $O_{2'}$ atom will attack at the P_1 atom with rich positive charge, which is more favorably than the attack at the C_β atom charged negatively, resulting in the priority of the P-path for HPpNP. On the other hand, the symmetry of molecular orbitalal is a decisive factor in the case of a chemical reaction. In the present work, we further investigated the features of the highest occupied molecular orbitals (HOMOs) of the reactants. The HOMOs of **O-RE_2** and **O-RE_1** are shown in Fig. 1-SI. It can be seen from the HOMO of **O-RE_2** that the orbitals of the $O_{2'}$ atom and the P_1 atom are symmetrical permission and overlap effectively. While for HOMO of **O-RE_1**, the orbitals of the $O_{2'}$ atom and the C_β atom are not compatible in symmetry apparently, hence they can not overlap effectively. Additionally, we found the transition state of the P-path is a five-membered ring for HPpNP while that of the C-path is a three-membered ring. It is obvious that the strained force of the five-membered ring is smaller than that of a three-membered ring,

which also implies that the P-path is more favorable than the C-path for HPpNP.

3.2. Intra-molecular attack of s-2′pNP

In this section, the results for the P-path and the C-path calculated for the reactions of s-2′pNP are presented. First, in order to model the experimental work, we choose the experimental system where there is not a methyl in the carbon atom near the $S_{2'}$. The optimized geometries and important bond lengths for the stationary points are shown in Fig. 2. Cartesian coordinates optimized in water are given in the Supporting information.

3.2.1. P-path

As described in Fig. 2a, a single transition state **S-TS$_P$** is found both in the gas phase and in solution for the P-path of s-2′pNP. The vector of the imaginary vibrational frequency (267.42 i cm^{-1}) in the transition state mainly corresponds to the bond formation between the nucleophilic $S_{2'}$ and P_1, and the bond cleavage to the nitrophenoxide leaving group. **S-TS$_P$** is a unique trigonal bipyramidal (TBP) structure. The $S_{2'}$—P_1 atomic distance is 2.580 Å, nearly 3 Å shorter than that of **S-RE**, corresponding to a natural bond order change from 0.003 (**S-RE**) to 0.385 (**S-TS$_P$**), The bond length of P_1—$O_{5'}$ of **S-TS$_P$** is about 0.5 Å longer than that of **S-RE**, corresponding to a bond order of 0.492 (**S-RE**) and 0.220 (**S-TS$_P$**). Compared with the P-path of HPpNP, the attacking and breaking bond length of **S-TS$_P$** are longer than that of **O-TS$_P$**, indicating that the transition state **S-TS$_P$** is looser than the **O-TS$_P$**.

E_v (%), E_{av} (%) and synchronicity (S_y) for the reactions are presented in Table 3. In the P-path for s-2′pNP, the P_1—$O_{5'}$ bond-breaking 55.28% are more advanced than $S_{2'}$—P_1 bond-attacking 52.11%. The E_v (%) values of the P-path for s-2′pNP are more advanced than that for HPpNP with the E_v (%) about 20%. It implies that the transition state of attacking the phosphorus atom for the s-2′pNP is later than that for the HPpNP, because the nucleophilicity of sulfur is weaker than that of oxygen. The similar results was obtained by Kim et al. [78] where the substituent effects in S_N2 reactions of benzyl chloride derivatives with phenoxides and thiophenoxides were carried out. The synchronicity value is 0.97 showing that the P-path process for the s-2′pNP is quite synchronous.

3.2.2. C-path

In the C-path for s-2′pNP, the $S_{2'}$ atom attacks the C_β atom to form the three-membered ring thiirane through a single transition state **S-TS$_C$** with one imaginary frequency of 438.11 i cm^{-1}. As depicted in Fig. 2b, the transition state **S-TS$_C$** features a concomitant bond formation between the nucleophilic $S_{2'}$ and C_β in s-2′pNP and the bond cleavage to the nitropheoxide leaving group. The former is evidenced by the shortening of the $S_{2'}$—C_β distance from 2.790 Å in RE to 2.262 Å at the saddle point, corresponding to a natural

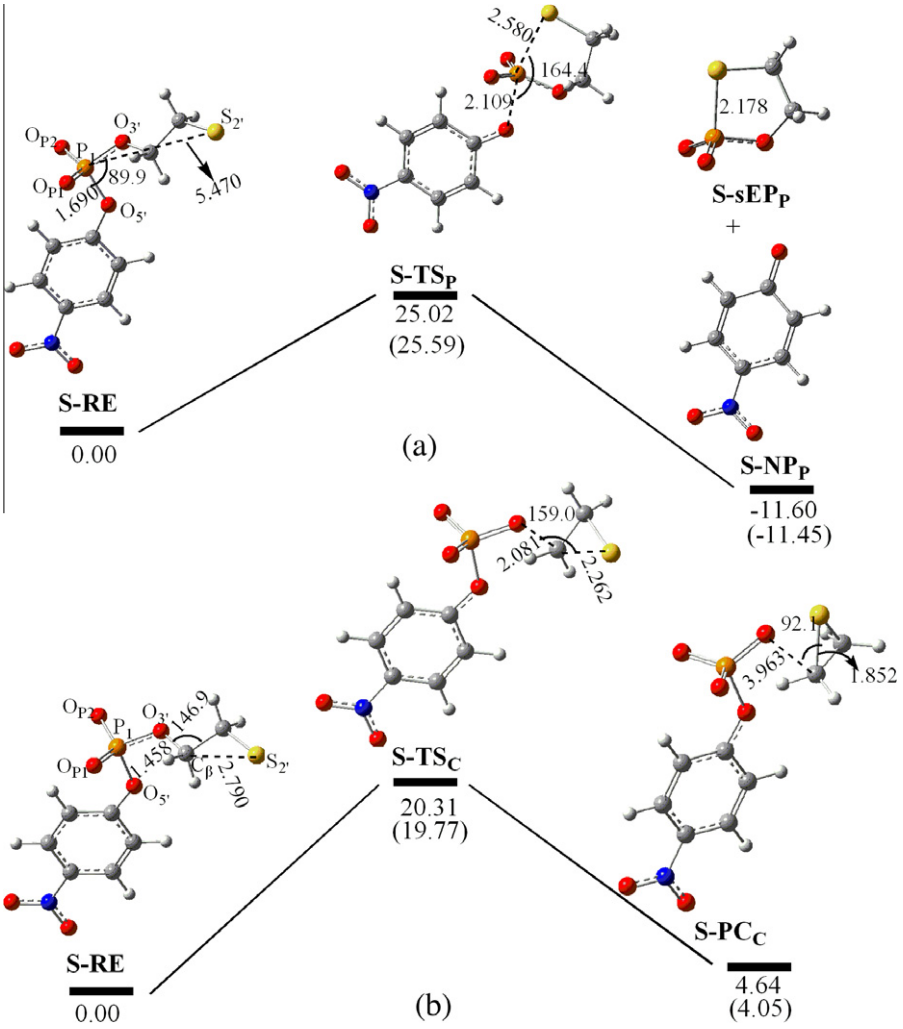

Fig. 2. B3LYP/6-31++G(df,p)-optimized structures (in Å) of the stationary points of s-2′pNP in the solution for the P-path (a) and the C-path (b), respectively. The values correspond to the relative free energy (ΔG) in kilocalories per mole. The values in parentheses are at the B3LYP/6-311++G(3df,2pd)//B3LYP/6-31++G(df,p) level.

bond order change from 0.051 (**S-RE**) to 0.483 (**S-TS$_C$**), and finally to 0.960 (**S-PC$_C$**). The latter is manifested by the elongation of the C_β—$O_{3'}$ bond from 1.458 Å in S-RE to 2.081 Å in **S-TS$_C$**, corresponding to a bond order of 0.844 (**S-RE**) and 0.333 (**S-TS$_C$**). These changes indicate the gradual breaking of the C_β—$O_{3'}$ bond and the yield of the product. In the final product **S-PC$_C$**, the $S_{2'}$—C_β bond distance shortens to 1.852 Å with Wiberg bond index 0.960, the C_β—$O_{3'}$ bond breaks completely and the corresponding Wiberg bond index decreases to 0.001. Compared with the C-path of HPpNP, the attacking and breaking bond length of **S-TS$_C$** are longer than that in the **O-TS$_C$**, indicating that the transition state **S-TS$_C$** is looser than the **O-TS$_C$**.

E_v (%), E_{av} (%) and synchronicity (S_y) for the reactions are presented in Table 3. In the C-path for s-2′pNP, the C_β—$O_{3'}$ bond-breaking 60.62% is more advanced than $S_{2'}$—C_β bond-attacking 47.52%. The synchronicity value is 0.88 showing that the C-path process is not as synchronous as the P-path for s-2′pNP.

3.2.3. Energy profile

The changes in energy including zero-point vibrational energy (ΔE_0), enthalpy of activation (ΔH) and Gibbs free energies (ΔG) for all the stationary points of s-2′pNP with respect to the reactant **S-RE** are given in Table 2.

For the P-path of s-2′pNP, the energy barrier is 24.19 kcal/mol and the free energy barrier is 24.40 kcal/mol in the gas phase. The entropic contributions tend to increase the energy barriers. Both the ΔE_0 and ΔG at the B3PW91/6-31++G(df,p) are similar to that at the B3LYP/6-31++G(df,p) level in the gas phase. The free energy barrier of the P-path decreases to 25.02 kcal/mol in solution, compared to 24.40 kcal/mol in the gas phase at B3LYP/6-31++G(df,p) level. Correspondingly, the free energy barrier decreases to 23.08 kcal/mol in solution, while it is 25.54 kcal/mol in the gas phase at B3PW91/6-31++G(df,p) level. When the single point energies were recalculated with PCM at the B3LYP/6-311++g(3df,2pd) and B3PW91/6-311++g(3df,2pd) levels, respectively, the ΔE_0 and ΔG become about 0.5 kcal/mol higher than the energies obtained with PCM at B3LYP/6-31++G(df,p) and B3PW91/6-31++G(df,p) levels. It can be seen from the energy profiles that the P-paths of s-2′pNP and HPpNP have the same trend with the considerations of the entropic contributions and the single point energy calculation with large basis sets.

For the C-path of s-2′pNP, the energy barrier is 20.71 kcal/mol and the free energy barriers are 19.82 kcal/mol in the gas phase. The entropic contributions tend to decrease the energy barriers. Both the ΔE_0 and ΔG at B3PW91/6-31++G(df,p) are higher than that at B3LYP/6-31++G(df,p) level. The bulk solvent effects are relatively small on the energy barrier of the C-path. When the single point energies were recalculated at B3LYP/6-311++G(3df,2pd) and B3PW91/6-311++g(3df,2pd) levels with PCM, the ΔE_0 and ΔG become slightly lower than those obtained with PCM at B3LYP/6-31++G(df,p) and B3PW91/6-31++G(df,p) levels. It also can be seen that the C-paths of s-2′pNP and HPpNP have the same trend with the considerations of the entropic contributions and the solvation. As depicted in Table 2, the free energy barrier in solution is about 21 kcal/mol. Accordingly, the rate constant of the C-path for s-2′pNP at 298.15 K is 0.00257 s^{-1}, which is close to the experimental value 0.00077 s^{-1} estimated from the half-time $t_{1/2}$ [56]. Similarly, the MP2 method increases the free energy barriers of two pathways. The free energy barriers ΔG for the P-path and C-path of s-2′pNP are 31.00 and 24.79 kcal/mol, respectively.

For s-2′pNP, the C-path, with the attack at the carbon atom is more favorable than the P-path, where the nucleophilic attack at the phosphorus atom. One can further infer that the 2′ thiouridyl group intra-molecular attack favors the formation of the products of the three-membered thriiane and a phosphomonoester characterized by C—O bond cleavage for s-2′pNP, which is consistent with the experimental work [56].

The NPA charge for the reactant of s-2′pNP is also presented in Table 1-SI. The NPA charge carried by the $S_{2'}$ atom for **S-RE** is −0.70e, which is 0.2e less than those of **O-RE$_2$** and **O-RE$_1$**, and the charges carried by the P_1 and C_β atom for **S-RE** are nearly the same as those of **O-RE$_2$** and **O-RE$_1$**. It seems that similar to HPpNP, the $S_{2'}$ atom should attack at the P_1 atom with rich positive charge, which implies the charge analysis can not provide a rational explanation for the reaction mechanism of s-2′pNP. While we found that the orbitals of the $S_{2'}$ atom and the C_β atom in **S-RE** are compatible in symmetry and can overlap effectively from the HOMO of **S-RE** shown in Fig. 1-SI. Next, we turn to the structures of the transition states. Because the atom radii of the sulfur atom is larger than that of the oxygen atom, the strained force of the three-membered ring of s-2′pNP decrease significantly, making the nucleophilic attack of the $S_{2'}$ atom at the beta carbon atom and the forming of the transition state with three-membered ring become probable.

Accordingly, the HPpNP and s-2′pNP exhibit dual electrophilic character: the hard nucleophile $O_{2'}$ atom with strong electronegativity attacks at the phosphorus charged positively more favorably than the beta carbon; while the soft nucleophile $S_{2'}$ atom attacks at the beta carbon, which is a ''soft'' electrophilic site, more favorably than at the phosphorus atom.

4. Conclusion

In this study, the intra-molecular attack of HPpNP and its analogous compound s-2′pNP with sulfur in the 2′ position have been studied using density functional theory method. The polarized continuum model (PCM) has been induced to account for the influence of solvation on the geometry structures in the reactions. The calculations show that the intra-molecular attack either with P—O bond cleavage or C—O bond cleavage for HPpNP and s-2′pNP proceeds through a S_N2 mechanism without any intermediate both in the gas phase and in solution. It is found that the P-path involving the five-membered ring cyclization of forming the methyl ethylene phosphate is more favorable than the C-path with the attack at the carbon atom both in the gas phase and in solution for HPpNP. While for s-2′pNP, the nucleophile $S_{2'}$ atom attacks at the beta carbon atom, with the forming of thiirane and a phosphomonoester undergoes C—O bond cleavage, leading to the C-path is more accessible than the P-path characterized by P—O bond cleavage. The calculated activation barriers of the favorable pathways for both HPpNP and s-2′pNP are in agreement with the experimental results. The results reveal that the C—O bond cleavage pathway should be taken into consideration for the thio effect of the phosphoryl transfer and hydrolysis of phosphate.

Acknowledgment

This work was supported by the National Natural Science Foundation of China (Grant No. 20973117).

Appendix A. Supplementary data

Supplementary data associated with this article can be found, in the online version, at doi:10.1016/j.bioorg.2011.09.003.

References

[1] F.H. Westheimer, Science 235 (1987) 1173–1178.
[2] D.M. Perreault, E.V. Anslyn, Angew. Chem., Int. Ed. Engl. 36 (1997) 432–450.
[3] M. Oivanen, S. Kuusela, H. Lönnberg, Chem. Rev 98 (1998) 961–990.
[4] (a) N. Usman, R. Cedergren, Trends Biochem. Sci. 17 (1992) 334–339;
(b) O. Heidenreich, W. Pieken, F. Eckstein, FASEB J. 7 (1993) 90–96;
(c) J.A. Grasby, C. Pritchard, M. Gait, Proc. Indian Acad. Sci. (1994) 1003–1022;

(d) D. Herschlag, F. Eckstein, T.R. Cech, Biochemistry 32 (1993) 8312–8321;
(e) O. Heidenreich, F. Benseler, A. Fahrenholz, F. Eckstein, J. Biol. Chem. 269 (1994) 2131–2138;
(f) B.E. Eaton, W.A. Pieken, Annu. Rev. Biochem. 64 (1995) 837–863;
(g) A. De Mesmaeker, R. Häner, P. Martin, H.E. Moser, Acc. Chem. Res. 28 (1995) 366–374.
[5] C.L. Dantzman, L.L. Kiessling, J. Am. Chem. Soc 118 (1996) 11715–11719.
[6] P. Molenveld, J.F. Engbersen, D.N. Reinhoudt, J. Org. Chem. 64 (1999) 6337–6341.
[7] L. Bonfá, M. Gatos, F. Mancin, P. Tecilla, U. Tonellato, Inorg. Chem. 42 (2003) 3943–3949.
[8] A.A. Neverov, Z.L. Lu, C.I. Maxwell, M.F. Mohamed, C.J. White, J.S. Tsang, R.S. Brown, J. Am. Chem. Soc. 128 (2006) (1639) 8–16405.
[9] Z.L. Lu, C.T. Liu, A.A. Neverov, R.S. Brown, J. Am. Chem. Soc. 129 (2007) 11642–11652.
[10] C.T. Liu, A.A. Neverov, R.S. Brown, Inorg. Chem 46 (2007) 1778–1788.
[11] Z.M. Zhang, Q.A. Fu, X.Q. Li, X. Huang, J.Y. Xu, J.C. Shen, J.Q. Liu, J. Biol. Inorg. Chem. 14 (2009) 653–662.
[12] A.J. Kirby, M. Younas, J. Chem. Soc. B (1970) 1165–1172.
[13] S.A. Ba-Saif, A.M. Davis, A. Williams, J. Org. Chem. 54 (1989) 5483–5486.
[14] A.C. Hengge, W.W. Cleland, J. Am. Chem. Soc. 112 (1990) 7421–7422.
[15] W.W. Cleland, A.C. Hengge, FASEB J. 9 (1995) 1585–1594.
[16] A.C. Hengge, A.E. Tobin, W.W. Cleland, J. Am. Chem. Soc. 117 (1995) 5919–5926.
[17] K.A. Maegley, S.J. Admiraal, D. Herschlag, Proc. Natl. Acad. Sci. USA 93 (1996) 8160–8166.
[18] S. Admiraal, D. Herschlag, J. Am. Chem. Soc. 122 (2000) 2145–2148.
[19] A.G. Cassano, V.E. Anderson, M.E. Harris, J. Am. Chem. Soc. 124 (2002) 10964–10965.
[20] J. Purcell, A.C. Hengge, J. Org. Chem. 70 (2005) 8437–8442.
[21] J.G. Zalatan, D. Herschlag, J. Am. Chem. Soc. 128 (2006) 1293–1303.
[22] C. McWhirter, E.A. Lund, E.A. Tanifum, G.Q. Feng, J. Am. Chem. Soc. 130 (2008) 13673–13682.
[23] M.E. Harris, Q. Dai, H. Gu, D.L. Kellerman, J.A. Piccirilli, V.E. Anderson, J. Am. Chem. Soc. 132 (2010) 11613–11621.
[24] J. Aqvist, A. Warshel, Biochemistry 28 (1989) 4680–4689.
[25] C. Lim, M. Karplus, J. Am. Chem. Soc. 112 (1990) 5872–5873.
[26] C. Lim, P. Tole, J. Phys. Chem. 96 (1992) 5217–5219.
[27] A. Dejaegere, M. Karplus, J. Am. Chem. Soc. 115 (1993) 5316–5317.
[28] J. Florián, A. Warshel, J. Am. Chem. Soc. 119 (1997) 5473–5474.
[29] J. Florián, A. Warshel, J. Phys. Chem. B 102 (1998) 719–734.
[30] X. Lopez, A. Dejaegere, M. Karplus, J. Am. Chem. Soc. 123 (2001) 11755–11763.
[31] G. Menegon, M. Loos, H. Chaimovich, J. Phys. Chem. A 106 (2002) 9078–9084.
[32] B.A. Gregersen, X. Lopez, D.M. York, J. Am. Chem. Soc. 125 (2003) 7178–7179.
[33] X. Chen, C.G. Zhan, J. Phys. Chem. A 108 (2004) 3789–3797.
[34] X. Chen, C.G. Zhan, J. Phys. Chem. A 108 (2004) 6407–6413.
[35] Y. Liu, B.A. Gregersen, X. Lopez, D.M. York, J. Phys. Chem. B 109 (2005) 19987–20003.
[36] G.A. Menegon, H. Chaimovich, J. Phys. Chem. A 109 (2005) 5625–5635.
[37] L.D. Zhang, D.Q. Xie, D.G. Xu, H. Guo, J. Phys. Chem. A 109 (2005) 11295–11303.
[38] Y. Liu, B.A. Gregersen, A. Hengge, D.M. York, Biochemistry 45 (2006) 10043–10053.
[39] X. Lopez, A. Dejaegere, F. Leclerc, J. Phys. Chem. B 110 (2006) 11525–11539.
[40] L.D. Zhang, D.Q. Xie, D.G. Xu, H. Guo, Chem. Commun. (2007) 1638–1640.
[41] E. Rosta, S.C. Kamerlin, A. Warshel, Biochemistry 47 (2008) 3725–3735.
[42] S.C. Kamerlin, M. Haranczyk, A. Warshel, ChemPhysChem 10 (2009) 1125–1134.
[43] S.C. Kamerlin, A. Warshel, J. Phys. Chem. B 113 (2009) (1569) 2–15698.
[44] B. Elsasser, G. Fels, Phys Chem Chem Phys 12 (2010) 11081–11088.
[45] F.H. Westheimer, Chem. Rev. 4 (1981) 313–326.
[46] H. Gilman, B. Gaj, J. Am. Chem. Soc. 82 (1960) 6326–6329.
[47] D.M. Brown, D.A. Usher, J. Chem. Soc. 87 (1965) 6558–6564.
[48] C.A. Bunton, Acc. Chem. Res. 3 (1970) 257–265.
[49] R.V. Hodges, S.A. Sullivan, J.L. Beauchamp, J. Am. Chem. Soc. 102 (1980) 935–938.
[50] R.C. Lum, J.J. Grabowski, J. Am. Chem. Soc. 114 (1992) 8619–8627.
[51] L.Y. Kuo, N.M. Perera, Inorg. Chem. 39 (2000) 2103–2106.
[52] B. Byczynski, S. Mizyed, P.J. Berti, J. Am. Chem. Soc. 125 (2003) 12541–12550.
[53] P.G. Loncke, P. Berti, J. Am. Chem. Soc. 128 (2006) 6132–6140.
[54] N. Ashkenazi, S.S. Zade, Y. Segall, Y.S. Kartona, M. Bendikov, Chem. Commun. (2005) 5879–5881.
[55] N. Ashkenazi, Y. Segall, Y. Karton, S.S. Zade, M. Bendikov, Phosphorus, Sulfur Silicon 183 (2008) 420–424.
[56] S. Iyer, A.C. Hengge, J. Org. Chem. 73 (2008) 4819–4829.
[57] D. Herschlag, J.A. Piccirilli, T.R. Cech, Biochemistry 30 (1991) 4844–4854.
[58] J.M. Galbraith, H.F. Schaefer, J. Chem. Phys. 105 (1996) 862–864.
[59] (a) M. Karplus, J. Phys. Chem. B 104 (2000) 11–27;
(b) R.A. Friesner, M.D. Beachy, Curr. Opin. Struct. Biol. 8 (1998) 257–262;
(c) A. Warshel, Annu. Rev. Biophys. Biomol. Struct. 32 (2003) 425–443.
[60] B.A. Gregersen, X. Lopez, D.M. York, J. Am. Chem. Soc. 126 (2004) 7504–7513.
[61] A.D. Beck, J. Chem. Phys. 98 (1993) 5648–5652.
[62] R.G. Parr, W. Yang, Density Functional Theory of Atoms and Molecules, Oxford University Press, Oxford, 1989.
[63] J.P. Perdew, Y. Wang, Phys. Rev. B 45 (1992) 13244–13249.
[64] A.D. Becke, J. Chem. Phys. 98 (1993) 1372–1377.
[65] C. Gonzalez, H.B. Schlegel, J. Chem. Phys. 90 (1989) 2154–2161.
[66] C. Gonzalez, H.B. Schlegel, J. Phys. Chem. A 94 (1990) 5523–5527.
[67] J. Tomasi, M. Persico, Chem. Rev. 94 (1994) 2027–2094.
[68] K.W. Wiberg, Tetrahedron 24 (1968) 1083–1095.
[69] A.E. Reed, J.E. Carpenter, F. Weinhold, NBO Version 3.1.
[70] M.J. Frisch, G.W. Trucks, H.B. Schlegel, G.E. Scuseria, M.A. Robb, J.R. Cheeseman, J. Montgomery, J.A.T. Vreven, K.N. Kudin, J.C. Burant, J.M. Millam, S.S. Iyengar, J. Tomasi, V. Barone, B. Mennucci, M. Cossi, G. Scalmani, N. Rega, G.A. Petersson, M. Nakatsuji, M. Hada, K. Ehara, R. Toyota, J. Fukuda, M. Hasegawa, T. Ishida, Y. Nakajima, Y. Honda, O. Kitao, H. Nakai, M. Klene, X. Li, J.E. Knox, H.P. Hratchian, J.B. Cross, C. Adacmo, J. Jaramillo, R. Gomperts, R.E. Stratmann, O. Yazyev, A.J. Austin, R. Cammi, C. Pomelli, J. Ochterski, P.Y. Ayala, K. Morokuma, G.A. Voth, P. Salvador, J.J. Dannenberg, V.G. Zakrzewski, S. Dapprich, A.D. Daniels, M.C. Strain, Farkas, D.K. Malick, A.D. Rabuck, K. Clifford, J. Cioslowki, B.B. Stefanov, G. Liu, A. Liashenko, P. Piskorz, I. Komaromi, R.L. Martin, D.J. Fox, T. Keith, M.A. Al-Laham, C.Y. Peng, A. Nanayakkara, M. Challacombe, P.M.W. Gill, B.G. Johnson, W. Chen, M.W. Wong, C. Gonzalez, J.A. Pople, Gaussian 03, Version D. 01, Gaussian, Inc., Pittsburgh, PA, 2005.
[71] M.Y. Yang, O. Iranzo, J.P. Richard, J.R. Morrow, J. Am. Chem. Soc. 127 (2005) 1064–1065.
[72] A.C. Hengge, W.W. Cleland, J. Am. Chem. Soc. 113 (1991) 5835–5841.
[73] A. Moyano, M.A. Pericàs, A. Valentí, J. Org. Chem. 54 (1989) 573–582.
[74] T. Humphry, S. Iyer, O. Iranzo, J.R. Morrow, J.P. Richard, P. Paneth, A.C. Hengge, J. Am. Chem. Soc. 130 (2008) (1785) 8–17866.
[75] A.P. Bento, F.M. Bickelhaupt, J. Org. Chem. 73 (2008) 7290–7299.
[76] W.J. Hehre, R. Ditchfield, J.A. Pople, J. Chem. Phys. 56 (1972) 2257–2261.
[77] M.S. Gordon, Chem. Phys. Lett. 76 (1980) 163–168.
[78] W.K. Kim, W.S. Ryu, I.S. Han, C.K. Kim, I. Lee, J. Phys. Org. Chem. 11 (1998) 115–124.